



HAL
open science

Characteristics of quasi-monochromatic ULF waves in the Venusian foreshock

Lican Shan, Christian Mazelle, Karim Meziane, Magda Delva, Quanming Lu, Yasong S. Ge, Aimin Du, Tielong Zhang

► **To cite this version:**

Lican Shan, Christian Mazelle, Karim Meziane, Magda Delva, Quanming Lu, et al.. Characteristics of quasi-monochromatic ULF waves in the Venusian foreshock. *Journal of Geophysical Research Space Physics*, 2016, 121, pp.7385-7397. 10.1002/2016JA022876 . insu-03675406

HAL Id: insu-03675406

<https://insu.hal.science/insu-03675406>

Submitted on 23 May 2022

HAL is a multi-disciplinary open access archive for the deposit and dissemination of scientific research documents, whether they are published or not. The documents may come from teaching and research institutions in France or abroad, or from public or private research centers.

L'archive ouverte pluridisciplinaire **HAL**, est destinée au dépôt et à la diffusion de documents scientifiques de niveau recherche, publiés ou non, émanant des établissements d'enseignement et de recherche français ou étrangers, des laboratoires publics ou privés.

Copyright

RESEARCH ARTICLE

10.1002/2016JA022876

Key Points:

- Properties of quasi-monochromatic ULF waves in the Venusian foreshock are determined
- The obtained results are very similar to the wave properties seen for ULF waves present in the terrestrial foreshock
- All the wave properties are consistent with generation by foreshock backstreaming ions

Correspondence to:

L. Shan and Q. Lu,
lcshan@mail.iggcas.ac.cn;
qmlu@ustc.edu.cn

Citation:

Shan, L., C. Mazelle, K. Meziane, M. Delva, Q. Lu, Y. S. Ge, A. Du, and T. Zhang (2016), Characteristics of quasi-monochromatic ULF waves in the Venusian foreshock, *J. Geophys. Res. Space Physics*, 121, 7385–7397, doi:10.1002/2016JA022876.

Received 28 APR 2016

Accepted 15 JUL 2016

Accepted article online 19 JUL 2016

Published online 8 AUG 2016

Characteristics of quasi-monochromatic ULF waves in the Venusian foreshock

Lican Shan^{1,2,3,4}, Christian Mazelle^{4,5}, Karim Meziane⁶, Magda Delva⁷, Quanming Lu^{1,4}, Yasong S. Ge², Aimin Du², and Tielong Zhang^{1,7}

¹CAS Key Laboratory of Geoscience Environment, Department of Geophysics and Planetary Science, University of Science and Technology of China, Hefei, China, ²Key Laboratory of Earth and Planetary Physics, Institute of Geology and Geophysics, Chinese Academy of Sciences, Beijing, China, ³Collaborative Innovation Center of Astronautical Science and Technology, Hefei, China, ⁴IRAP, CNRS, Toulouse, France, ⁵IRAP, University Paul Sabatier, Toulouse, France, ⁶Department of Physics, University of New Brunswick, Fredericton, New Brunswick, Canada, ⁷Space Research Institute, Austrian Academy of Sciences, Graz, Austria

Abstract The statistical properties of ULF waves observed upstream of Venus foreshock are investigated. The study is restricted to waves which are observed well below the local proton cyclotron frequency. Using the magnetic field observations from Venus Express between May 2006 and February 2012, 115 quasi-monochromatic ULF wave trains have been identified. Statistical results show that the wave periods are mainly from 20 to 30 s in the spacecraft frame, which is about 2–3 times of the local proton cyclotron period. The transverse power dominates the power spectrum, and most of the waves display nearly circular or slightly elliptical polarization in the spacecraft frame. Moreover, these ULF waves mainly have small relative amplitudes with respect to the ambient field magnitude B_0 for parallel component ($\delta B_{\parallel}/B_0$ less than 0.3), while the range of relative amplitudes for perpendicular component $\delta B_{\perp}/B_0$ is from ~ 0.1 to ~ 1.0 . Wave propagation angles are mainly less than 30° with respect to the mean magnetic field direction. The obtained results are very similar to the wave properties seen for ULF waves present in the terrestrial foreshock, which suggests that backstreaming ions in the Venusian foreshock form an important energy source for the generation of the waves.

1. Introduction

A planetary bow shock and its subsequent related foreshock region are significant physical phenomena inherent to a planet immersed in the solar wind plasma. In the foreshock region of Earth, a significant wave activity associated with backstreaming particles is observed [Hoppe *et al.*, 1981; Russell and Hoppe, 1983; Thomsen *et al.*, 1985; Wilson, 2016, and references therein]. The foreshock region is bounded by the shock surface and the interplanetary magnetic field line, which is tangent to the latter. This region has different physical properties compared to the pristine solar wind. Particles emanating from the shock are subject upstream to the drift resulting from the convective solar wind electric field. Faster particles will be found backstreaming more upstream comparatively to the slower ones. Due to this velocity filtering, the electrons will be seen first from the tangent line boundary, while the ions are observed further downstream inside the ion foreshock boundary.

Upstream of the Earth's bow shock, several different types of backstreaming ion distributions, including field-aligned (termed reflected in earlier literature), gyrating, intermediate, and diffuse ions, have been identified from early spacecraft observations [Gosling *et al.*, 1978; Paschmann *et al.*, 1981; Fuselier, 1995]. Field-aligned beam distributions are usually seen from the quasi-perpendicular region to oblique regions, and their energy is from few to several keV [Paschmann *et al.*, 1980; Bonifazi and Moreno, 1981; Kucharek *et al.*, 2004; Meziane *et al.*, 2005]. Detailed investigations indicate that their thermal energy is controlled by the solar wind thermal energy and the shock geometry [Meziane *et al.*, 2013]. Observed downstream from the field-aligned beam source region, intermediate and gyrating ion distributions are usually thought to arise from field-aligned distributions through the nonlinear wave-particle interaction [Winske and Leroy, 1984; Hoshino and Terasawa, 1985; Mazelle *et al.*, 2000, 2003]. Under rare interplanetary magnetic field (IMF) conditions, both field-aligned beams and gyrating ions can be observed simultaneously due to the finite gyroradius effect of the latter (gyrating ions) [Meziane *et al.*, 2004a]. This simultaneous observation occurs when the spacecraft crosses the boundary between the two populations. Gyrating and intermediate ion distributions may also emanate from the quasi-parallel shock [Gosling *et al.*, 1982; Meziane *et al.*, 2004b]. The production mechanisms of both

field-aligned beams and gyrating ions have also been investigated by numerical studies [Burgess, 1987; Gedalin et al., 2008; Savoini and Lembège, 2015], which relate both field-aligned and gyrating distributions to the same reflection process at the shock. Finally, diffuse ion distributions originate from ion reflection or scattering at the quasi-parallel shock region [Fuselier, 1995; Scholer, 1995; Su et al., 2012]. They also may result from field-aligned beam disruption [Paschmann et al., 1981].

Inside the foreshock, the interaction of backstreaming particles with solar wind ions excites a variety of wave activities. Several distinct wave modes are observed in the terrestrial foreshock [Orlowski et al., 1990; Le and Russell, 1994; Greenstadt et al., 1995; Burgess, 1997; Blanco-Cano et al., 1999]. The so-called '30s' (typical period in the spacecraft frame) ultralow frequency (ULF) wave is one of a main type of wave activity, and it has been extensively observed in the Earth's foreshock [Hoppe and Russell, 1983; Thomsen et al., 1985; Meziane et al., 2001; Mazelle et al., 2003; Eastwood et al., 2005a, 2005b; Wilson et al., 2013] and other terrestrial bodies including Venus [Russell and Hoppe, 1983; Orlowski et al., 1994; Shan et al., 2014], Mars [Mazelle et al., 2004], Saturn [Orlowski et al., 1995; Bertucci et al., 2007; Andrés et al., 2013], and Mercury [Le et al., 2013], and also at quasi-perpendicular interplanetary shocks [Wilson et al., 2009]. Hoppe and Russell [1982] also found that there is a linear trend between wave frequency and ambient magnetic field strength for the different planets.

About the typical upstream parameters for the Venusian bow shock, the solar wind conditions at 0.72 AU based on Pioneer Venus Orbiter (PVO) observations [Russell et al., 2006] give a average value of plasma beta of 0.66 and a fast magnetosonic Mach number at the subsolar point of 4.2 for solar maximum case, while the corresponding numbers are 2.5 and 5.6 for the solar minimum case (from the website <http://ppi.pds.nasa.gov/>).

Linear theory and numerical simulations results reveal that field-aligned beams are the most efficient population to drive the ion/ion electromagnetic right-hand resonant mode unstable compared to other foreshock ion distributions [Gary et al., 1981; Gary, 1991; Winske and Quest, 1986; Mazelle et al., 2003; Lu et al., 2006, 2009]. Global hybrid simulations show that the sinusoidal quasi-monochromatic ULF waves are generated by field-aligned beams [Blanco-Cano et al., 2006a]. Due to solar wind convection, the produced waves are blown back to the shock causing significant changes of its structure [Blanco-Cano et al., 2006b]. Mazelle et al. [2005, 2007] have shown from Cluster observations that the ULF waves are generated by field-aligned beams at the inner edge of the gyrating ion regions and that during wave-particle interaction these beams have evolved into gyrophase-bunched ions.

Using ISEE 1 and 2 data, Hoppe and Russell [1983] identified sinusoidal ULF waves upstream of the Earth bow shock and that these waves are magnetosonic with frequency about 0.1 times of ion cyclotron frequency and wavelength $\sim 1 R_E$ in the solar wind rest frame. The waves are right-hand polarized in solar wind rest frame but appear left-hand polarized in the spacecraft frame because of the Doppler shift. Benefiting from multiple spacecraft analysis, recent statistical investigations presented more accurate results [Eastwood et al., 2005a], which have shown that the quasi-monochromatic ULF waves have an average period of 31 s in the spacecraft frame, a wavelength of about $1.5 R_E$, and the mean propagation angle with the ambient field is about 21° .

Based on two ULF wave events with similar IMF conditions, a previous study [Le and Russell, 1992a] indicated that the power spectrum of ULF wave in the deeper foreshock appeared broader than a wave near the foreshock boundary, and the wave amplitude and polarization were also different. Larger amplitude and higher compressional waves were interpreted as a further evolution of less compressional and lower amplitude waves [Hoppe and Russell, 1983]. Numerical simulations suggested that sinusoidal waves and highly compressive fluctuations are present at different positions and associated with different type of foreshock ion distributions [Blanco-Cano et al., 2006a]. The observed frequency in the spacecraft frame has a bandwidth due to the Doppler shift associated with the solar wind speed and its variations. Moreover, the bandwidth in the spacecraft frame will be larger for oblique propagations.

ULF wave activity has also been reported upstream of Venus bow shock. Russell and Hoppe [1983] identified one ULF wave case with a frequency of ~ 0.03 Hz. Another detailed case study revealed a transverse ULF wave, with wave power peak at 0.08 Hz and frequency band less than 0.04 Hz, an amplitude of ~ 1.2 nT, left-hand elliptically polarized in the spacecraft frame, and a propagation angle of 12° from ambient magnetic field [Orlowski et al., 1995]. Near the Venusian bow shock, Shan et al. [2014] identified five quasi-monochromatic

ULF wave events originating from the upstream of the quasi-parallel shock and which seem to have been transmitted downstream. These waves were found to have similar properties in the foreshock and magnetosheath: frequency 0.04–0.05 Hz in spacecraft frame, an average oblique propagation angle of $\sim 32^\circ$, left-handed elliptical polarization, and large amplitude, indicating that the waves are magnetosonic waves, which are blown from upstream to downstream by the solar wind.

Recent observational studies have shown that there are proton cyclotron waves which are excited by newborn protons through ion/ion resonant instability in the upstream region of Venus [Delva *et al.*, 2008, 2011]. Those waves occur mainly downstream of the terminator plane because of higher density of newborn ions in that region [Delva *et al.*, 2015]. Their frequency in the spacecraft frame is exactly at the local proton gyrofrequency (with less than 20% deviation), which is much higher than for the foreshock ULF waves generated by backstreaming ions. Moreover, the foreshock ULF waves are only observed when the IMF lines are connected to the bow shock on the contrary to the proton cyclotron waves seen everywhere in the upstream region of the bow shock.

For the present work, we investigate the statistical properties of quasi-monochromatic foreshock ULF waves observed upstream of the Venusian bow shock by using 1 Hz magnetic field measurements from Venus Express [Zhang *et al.*, 2006]. One important aim of the present study is to compare the terrestrial foreshock with the Venusian one.

Although, Venus' size is similar to that of Earth, the lack of a global magnetic field may induce differences that could be instructive. Many differences can be expected for the shock and the foreshock at Venus compared to the terrestrial case (magnetized planet) for nearly the same planet size. First, the standoff distance of the Venusian bow shock is much less than the planetary radius. The first consequence is that it makes the relative value of the curvature radius of the shock compared to the upstream solar wind proton gyroradius much smaller particularly on the dayside compared to the Earth case. This may influence the reflection mechanisms of the particles, which are the source of the ULF waves, and the particle properties can differ from what is expected by analytical calculations assuming a locally planar shock. Second, that makes the size of the bow shock and associated foreshock much smaller. Thus, the instabilities have much less time and space to grow, propagate, and evolve through the wave-particle interaction processes.

2. Measurements and Wave Selection

Venus Express was launched on 9 November 2005 and arrived in the Venus orbit on 11 April 2006. The spacecraft has an elliptical polar orbit (period 24 h) with a periapsis of 250–300 km and an apoapsis of $\sim 12 R_V$ (Venus radius 6052 km); this allowed two bow shock crossings per orbit. The orbital plane is fixed in space and therefore performs a full rotation through the plasma regions in one Venusian year. Magnetic field data with 1 Hz data rate are available throughout the full orbit [Zhang *et al.*, 2006].

First, the bow shock crossings are identified, which allow us to distinguish the measurements in the foreshock from the magnetosheath. In the solar wind, the typical value of magnetic field is about 7 nT. Due to lack of reliable plasma data, a precise determination of solar wind parameters is not possible. Based on Shan *et al.*'s [2015] bow shock model, the angles θ_{Bn} (angle between IMF and shock normal) can be estimated. In the VSO system of coordinates, x axis points to the Sun, y axis is oriented along the Venusian orbital velocity, and z axis completes the right-hand system. The magnetic field data in VSO (Venus Solar Orbital) frame are transformed into mean field coordinates defined as follows: z axis is along the direction to mean magnetic field (averaged over an arbitrarily defined time interval), y axis is perpendicular to z axis and VSO x axis, and x axis completes the right-handed coordinated set. Therefore, the compressional magnetic field component is given by the parallel component (B_z) in the mean field system and the transverse component vector is easily derived from the difference between each magnetic field vector and the parallel component. In order to identify quasi-monochromatic ULF waves, an automatic survey on the MAG data from May 2006 to February 2012 is realized. A fast Fourier transform (FFT) procedure is performed on each 10 min data interval (lowest frequency of ~ 0.00167 Hz). The time interval should be chosen long enough to contain a sufficient number of wave periods in order to compute a reliable power spectral density by using FFT while allowing to compute an average magnetic field providing a good quantitative estimate of the local ambient field. This is required to obtain physically reliable parallel and transverse wavefield components. However, the time interval must not be too long to avoid variations of the ambient field. Different time intervals have been tried,

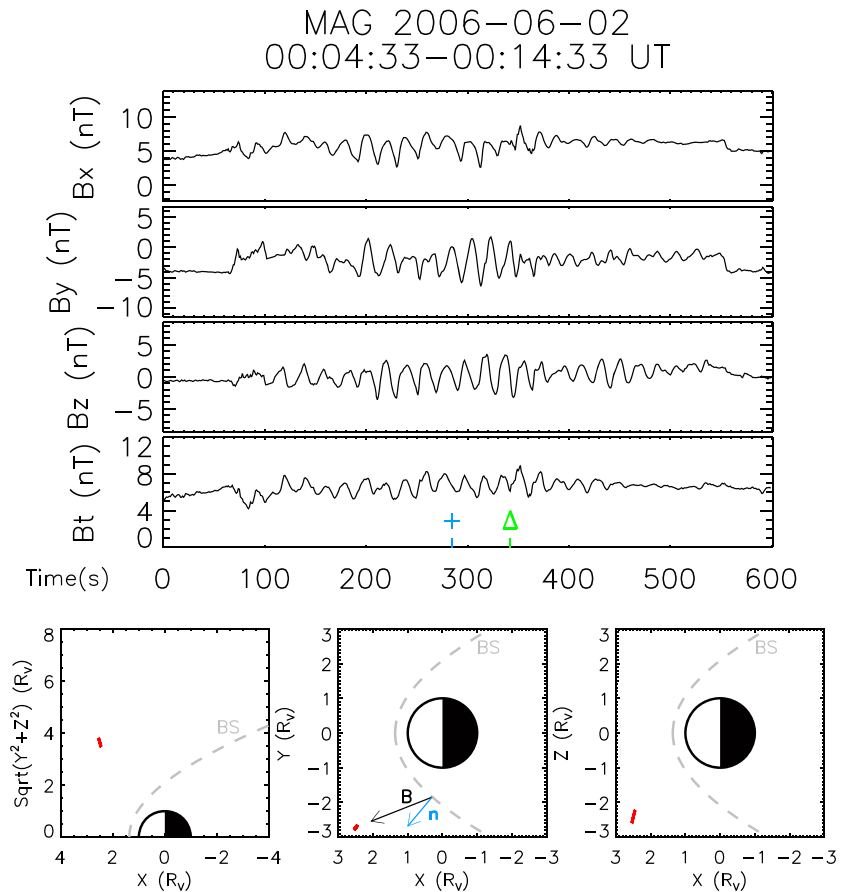


Figure 1. ULF wave occurrence in the Venusian foreshock observed by Venus Express on 2 June 2006. The subinterval marked by the plus-minus sign and triangle is used in Figure 2. (bottom row) The part of the VEX orbit during the wave observations is also shown in red line. The dashed lines represent the model bow shock. In Figure 1 (bottom middle), the projections of interplanetary magnetic field and shock normal are also plotted.

and the chosen one appeared to be appropriate. The compressional and transverse power parts are separated, and the local proton cyclotron frequency f_{cp} (~ 0.1 Hz for typical magnetic field value) is calculated. The wave events that fulfill the following criteria on the dominating power part are selected:

1. In the frequency range 0.012 Hz–0.1 Hz or 0.012 Hz– f_{cp} (with $f_{cp} < 0.1$ Hz), there is only one power peak whose frequency is equal or less than $2/3 f_{cp}$. At this point, we verify that the lower limit of frequency range (0.012 Hz) is higher than the lowest frequency in the FFT procedure and the peak frequency is sufficiently lower than the local f_{cp} , because our aim is to exclude proton cyclotron waves.
2. Near the peak power P_{max} , the frequency band corresponding to limit frequencies f_{min} and f_{max} for which the power spectral density is equal to $0.3 P_{max}$. The frequency band should have a very narrow range that is equal to or less than 0.010 Hz in the present investigation. That means, only the quasi-monochromatic ULF waves are selected by this survey.
3. The identified peak should be associated with a sufficiently strong power, which is about at least 2 times larger than its neighbor power.

3. Data Analysis and Statistical Results

Using an automatic survey, we identified a total number of 115 quasi-monochromatic wave trains, which included 157 events of 10 min. In the case where the interval between two selected subintervals is 3 times larger than the wave period, we consider those cases as two distinct events. A case event is first analyzed. Figure 1 shows magnetic field measurements (B_x , B_y , and B_z components in VSO frame) on 2 June 2006. Figure 1 (bottom row) show the spacecraft positions (red line) and here adopted model bow

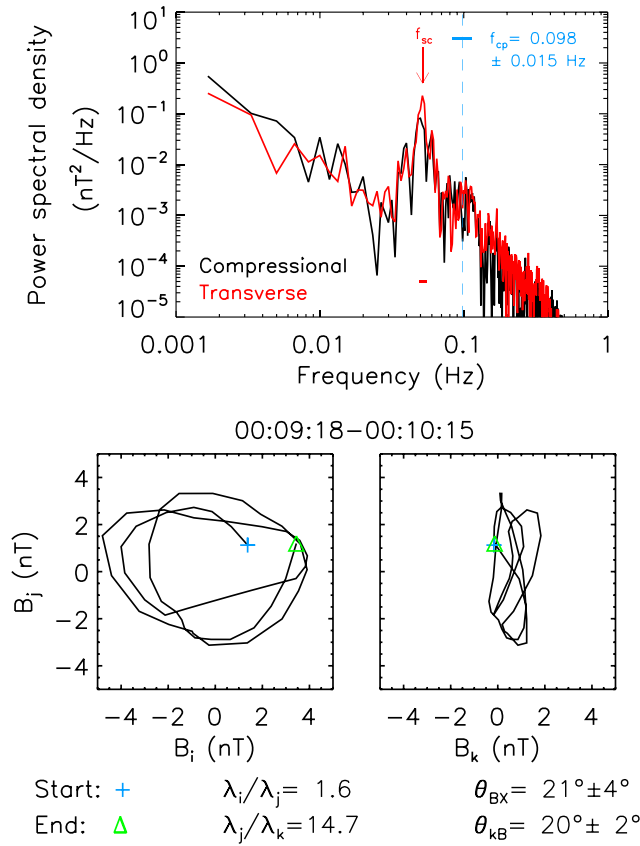


Figure 2. Wave power spectrum for compressional (black) and transverse (red) magnetic field components and hodograms of the ULF wave case on 2 June 2006. The red arrow and blue dashed line mark the peak frequency for the maximum power and local proton gyrofrequency, respectively, with the associated error bars. (bottom) The hodograms from MVA of a subinterval with length ~ 3 wave periods. The plus-minus sign and triangle indicate the start and end of the subinterval, respectively.

dashed line) $f_{cp} = 0.098 \pm 0.015$ Hz, which is about 1.9 times the peak frequency. It is clear that the transverse part dominates the power spectrum around the peak frequency. The minimum variance analysis (MVA) method [Sonnerup and Scherble, 1998] is used for hodograms analysis in principal axis coordinates [Rankin and Kurtz, 1970; McPherron et al., 1972]. Here a subinterval of about 3 times the wave period is selected for the MVA. The underscripts i, j , and k refer to the maximum, intermediate, and minimum variance eigenvalues, respectively, as well the associated principal axes and eigenvectors; B_i and B_j are the magnetic field components in the wave plane, while B_k is parallel (or antiparallel) to the wave propagation direction. The plus-minus sign and triangle on the (B_i, B_j) hodogram indicate the start and end of the analyzed interval, respectively. It results from the MVA technique that the ratios of the maximum to intermediate (λ_i/λ_j) and intermediate to minimum (λ_j/λ_k) eigenvalues are 1.6 and 14.7, respectively. The prior ratio describes the polarization of the wave: a value close to 1 means circular polarization, while larger values mean elliptical or even linear polarization for very large ones. Therefore, the obtained value of $\lambda_i/\lambda_j (=1.6)$ indicates a nearly circular or slightly elliptical polarization. The latter ratio provides an estimation of the uncertainty on the wave propagation direction [Sonnerup and Scherble, 1998], and the larger this value, the smaller this uncertainty. Usually, a numerical value larger than 5 stipulates that the entailed error is not significant. The obtained value for the present case is obviously large enough for a reliable analysis. In the $B_i - B_j$ plane, the ambient magnetic field points into the plane. Therefore, the apparent polarization in the spacecraft frame is left-handed with respect to the average magnetic field. We found that the IMF cone angle (the angle between the average magnetic field and x axis of VSO system) $\theta_{Bx} = 21^\circ \pm 4^\circ$, and the angle between the wave propagation direction and the

shock (dashed line) from Shan et al. [2015]. During the time interval of interest, the spacecraft moved from the position $(2.54, -2.78, -2.59) R_V$ to $(2.45, -2.67, -2.22) R_V$ in the upstream region, and the IMF is nearly in the x - y plane of VSO frame. Because of the unavailability of plasma data, we are unable to adjust the Venusian bow shock according to the ram pressure when VEX observed the waves in the foreshock region. Figure 1 (bottom middle) shows the projection of the IMF field (black arrow) and the shock normal (blue arrow), computed from the bow shock model; it appears that the wave interval is located well inside the foreshock region. The IMF direction makes an angle $\theta_{Bn} \sim 26^\circ$ with the shock normal, indicating a quasi-parallel geometry. Finally, based on the used bow shock and at the time of interest, VEX spacecraft is located at $\sim 2.4 R_V$ from the bow shock.

Figure 2 shows the power spectrum, separated into the transverse (red) and compressional (black) parts, and hodograms for a subinterval (from 00:09:18 to 00:10:15 UT indicated by the plus sign and triangle on Figure 1) of the wave shown in Figure 1. The peak frequency of the waves (indicated by the red arrow) $f_{sc} = 0.051 \pm 0.003$ Hz in the spacecraft frame, and the local proton cyclotron frequency (marked by the

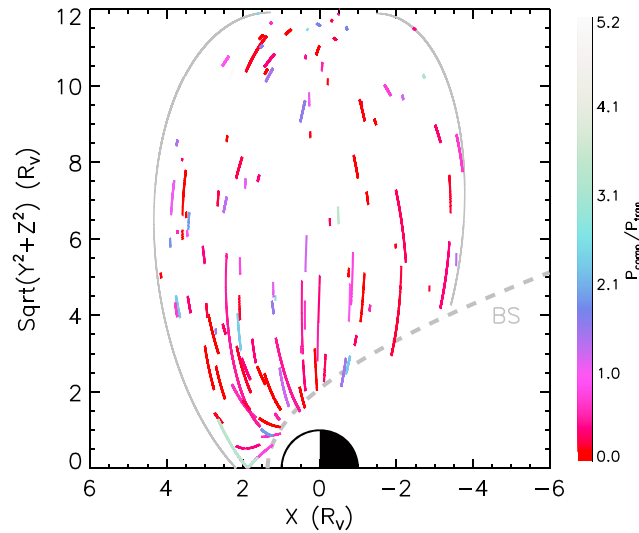
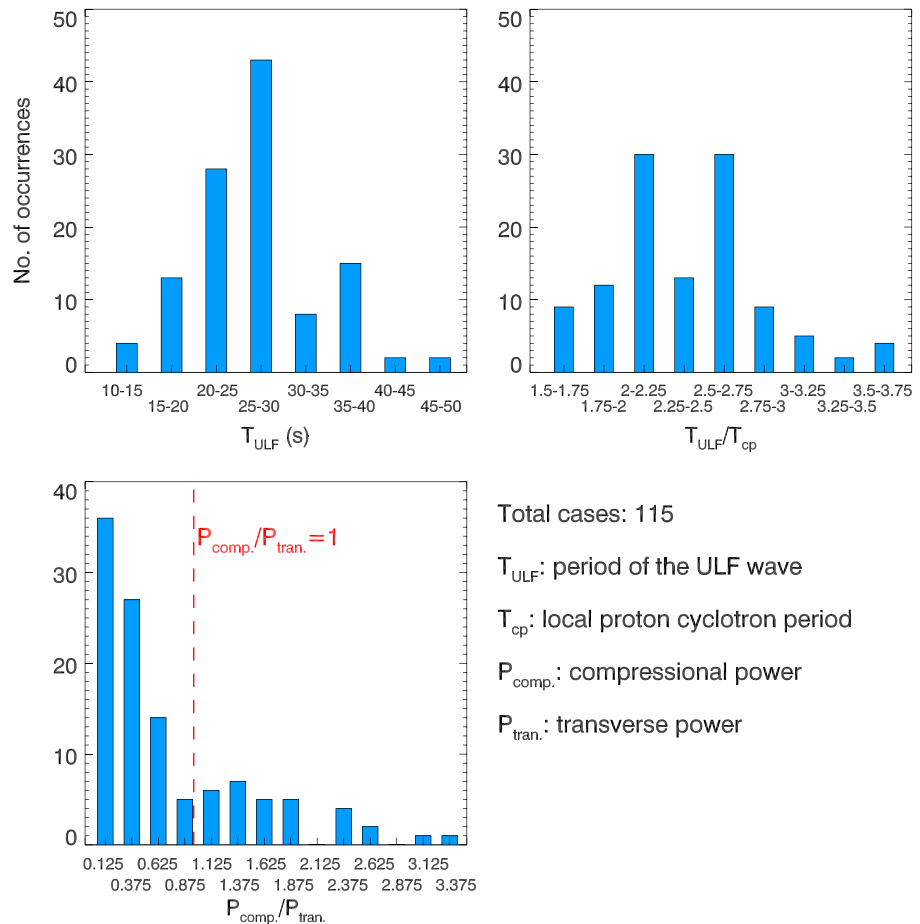


Figure 3. Spatial distributions of observations of 115 ULF wave trains in the VSO cylindrical coordinates. The grey curves are the orbit limits, and VEX cannot go outside of this region. The dashed line indicates the model bow shock. The color coding is corresponding to the ratios of compressional to transverse power of the waves.

ambient magnetic field $\theta_{kB} = 20^\circ \pm 2^\circ$. It appears that the wave propagation direction is nearly parallel to the ambient magnetic field and near the x axis. Assuming a solar wind speed of 450 km/s, an estimation of the wavelength can be obtained; we found $\lambda \sim 1.35 R_V$. This appears very similar to the typical values seen in the case of the Earth foreshock.

We now present the statistical results as based on the automatic identification of ULF waves; 115 cases are found between May 2006 and February 2012. Figure 3 shows the location of all the considered wave trains upstream of Venus bow shock. The dashed grey line represents the model bow shock, while the grey lines indicate the limiting orbits of the spacecraft. These observations indicate that the waves can be present



Total cases: 115
 T_{ULF} : period of the ULF wave
 T_{cp} : local proton cyclotron period
 $P_{comp.}$: compressional power
 $P_{tran.}$: transverse power

Figure 4. Histograms of 115 ULF waves. (top) The period and ratio period to local proton cyclotron period. (bottom) The histogram of ratios of compressional to transverse power.

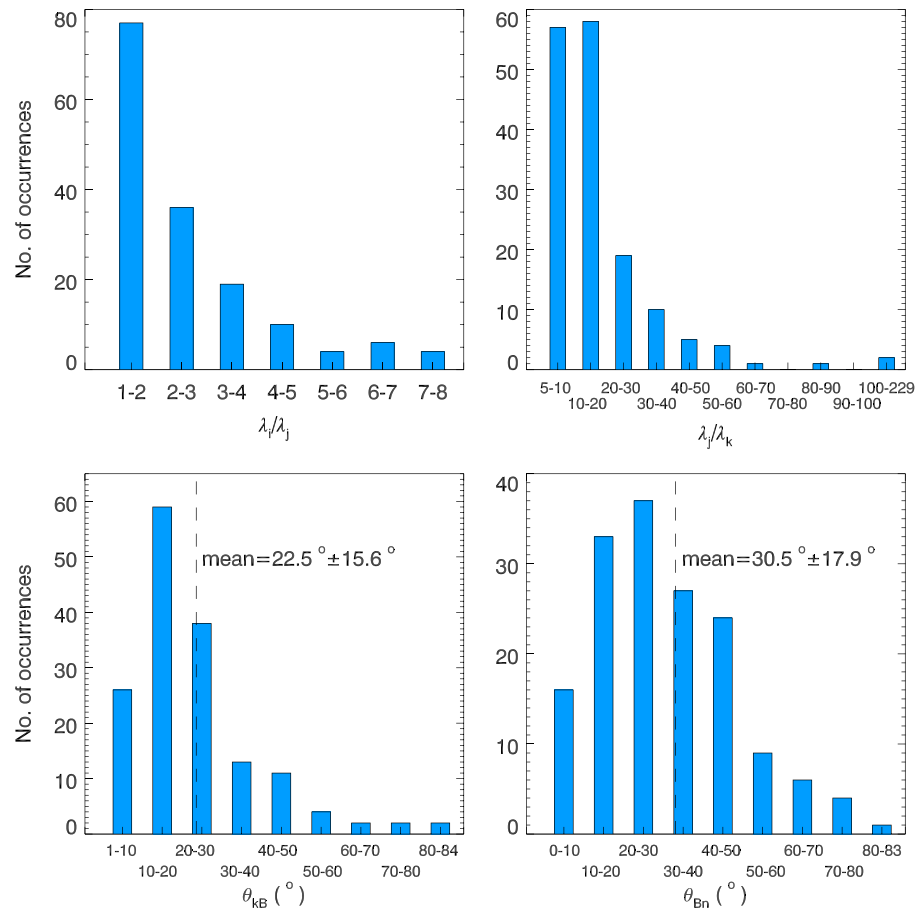


Figure 5. Histograms of 157 ULF waves’ parameters obtained from MVA method. (top) Eigenvalue ratios; (bottom left) wave propagation angles and (bottom right) shock normal angles.

in all the foreshock regions accessible by the spacecraft and up to large distances near the apoapsis (~12 R_V). Moreover, most of the cases are observed upstream of the terminator plane. These results are very different from proton cyclotron waves investigated by *Delva et al.* [2015], who found more events downstream of the terminator plane.

Figure 4 provides the ULF wave statistical properties obtained from our analysis. The wave period in second of time (Figure 4, top left) and normalized to the proton cyclotron period— T_{cp} (Figure 4, top right) distributions is shown. Most of ULF waves (~62%) have a 20–30 s period, which is about $2 - 3 \times T_{cp}$. Figure 4 (bottom) shows the histogram of the compressional to transverse power ratio; it indicates that 71% of the waves are dominated by the transverse part (i.e., $P_{comp}/P_{tran} < 1$). The color coding in Figure 3 shows the P_{comp}/P_{tran} ratio values. We find that the transverse waves occur in all the foreshock regions. Even near the bow shock, there are waves with weaker compressional parts.

The specific wave properties, obtained with the MVA technique, are shown in Figure 5. Only events with ratios of intermediate to minimum (λ_j/λ_k) eigenvalues larger than 5 for which errors on θ_{kB} is less than 10° are considered. The top histograms show the ratios of the maximum to intermediate (λ_i/λ_j) and intermediate to minimum (λ_j/λ_k) eigenvalues. Most of the ratios (λ_i/λ_j) are close to 1, which illustrates that the waves have mainly a nearly circular or slightly elliptical polarization. Simultaneously, the ratios (λ_j/λ_k) are sufficiently large (with 64% cases > 10) indicating a high reliability of the MVA method. Even under stringent conditions ($\lambda_j/\lambda_k > 10$), the histogram would be very similar (not shown here). Figure 5 (bottom left) shows the distribution of wave propagation angle θ_{kB} ; we found a mean value equals to $22.5^\circ \pm 15.6^\circ$. Most angles (~78%) are less than 30° .

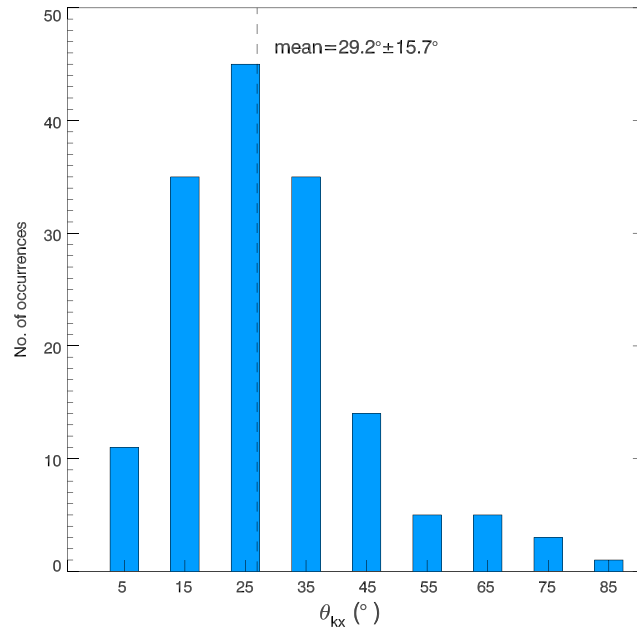


Figure 6. Histogram of 157 ULF waves' angle between the wave propagation directions obtained from MVA method and the X-VSO axis, assuming propagation toward the Sun.

The shock normal angles θ_{Bn} associated with each event is also determined: we obtained a mean value of $\theta_{Bn} = 30.5^\circ \pm 17.9^\circ$. It is clear that most of the waves are observed in the quasi-parallel foreshock region ($\theta_{Bn} < 45^\circ$).

Figure 6 displays the histogram of the angle θ_{kx} between the wave vector and the x axis of the VSO system forcing this angle to be between 0 and 90° (using only $|\mathbf{e}_{kx}|$ where \mathbf{e}_{kx} is the eigenvector associated with the minimum variance). This gives an indication of the angle between the direction of propagation and the solar wind velocity which plays an important role in the Doppler shift between the plasma rest frame and the spacecraft frame: we find a mean value of $\theta_{kx} = 29.2^\circ \pm 15.7^\circ$. It is clear that for most of the waves $\pm \mathbf{k}$ is not at a large angle with respect to the solar wind velocity vector, which implies a strong Doppler shift.

Figure 7 shows the spatial distributions of waves as a function of the same parameters as in Figure 5: λ_i/λ_j (Figure 7, top left), λ_j/λ_k (Figure 7, top right), θ_{kB} (Figure 7, bottom left), and associated θ_{Bn} (Figure 7, bottom right). In Figure 7 (top left), circularly or slightly elliptical polarized waves were observed everywhere in the

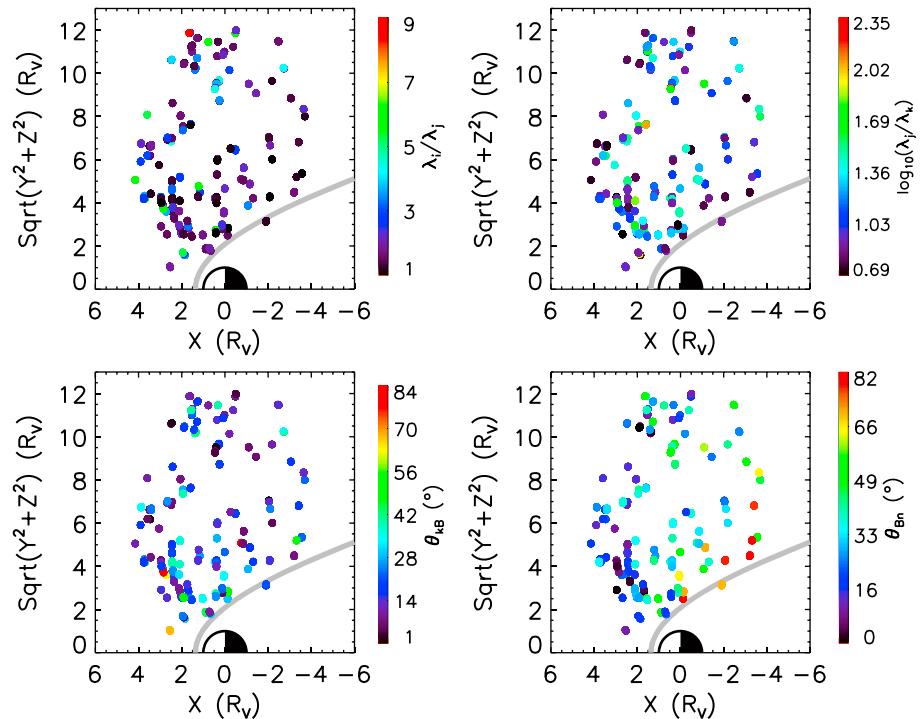


Figure 7. Spatial distribution of 157 ULF wave intervals in the VSO cylindrical coordinates for (top left) λ_i/λ_j , (top right) λ_j/λ_k , (bottom left) θ_{kB} , and (bottom right) θ_{Bn} .

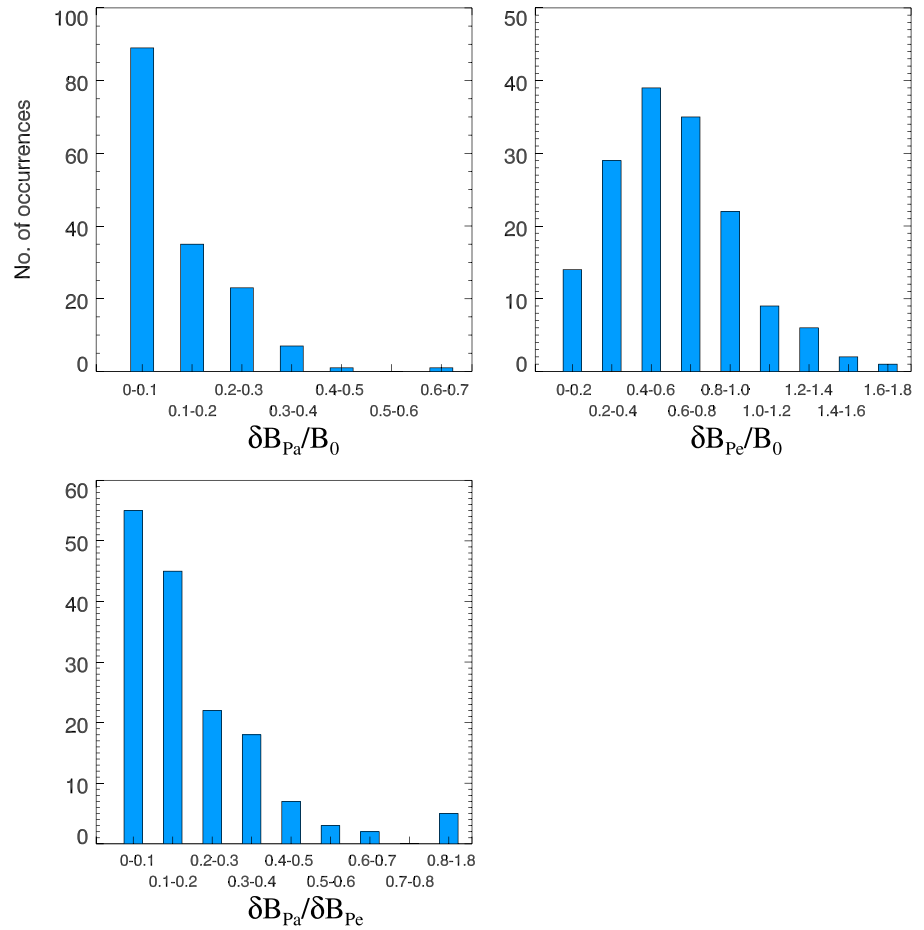


Figure 8. Histograms of the (top left) parallel and (top right) perpendicular amplitudes and (bottom left) the ratios between them from 157 selected subintervals as same as Figure 5.

foreshock, and several wave cases with more elliptical polarizations (larger λ_i/λ_j , marked by red or green color) appear mainly at further distance from the shock. While for θ_{kB} , more oblique propagation is observed when closer to the shock and relatively more distant upstream from the terminator, but it usually corresponds to low λ_i/λ_j . Cases associated with large θ_{Bn} appear mostly downstream from the terminator.

Finally, we calculated the relative wave amplitude components (Figure 8) $\delta B_{pa}/B_o$ and $\delta B_{pe}/B_o$, respectively, for wave events with $\lambda_j/\lambda_k > 5$ and errors on $\theta_{kB} < 10^\circ$; δB_{pa} (δB_{pe}) is the parallel(perpendicular) wave amplitude component and B_o is the average magnetic field. The amplitude components are calculated as follows:

$$\begin{aligned} \delta \mathbf{B}(t) &= \mathbf{B}(t) - \mathbf{B}_o \\ \delta \mathbf{B}_{pa}(t) &= \mathbf{B}_{pa}(t) - \mathbf{B}_o \\ \delta \mathbf{B}_{pe}(t) &= \delta \mathbf{B}(t) - \delta \mathbf{B}_{pa}(t) \end{aligned} \tag{1}$$

here t indicating the time series and the boldface represent vectors. For the parallel and perpendicular components of each wave event, we calculated errors for each case. Figure 9 displays the histogram of the errors for them

$$\frac{\left| \sqrt{\delta B_{pa}^2 + \delta B_{pe}^2} - \delta B \right|}{\delta B}$$

where δB is the mean amplitude of a wave event. The error on the determination of the amplitudes may come from the deviation of the computed B_o . It appears on Figure 8 that most waves (~94%) have small relative

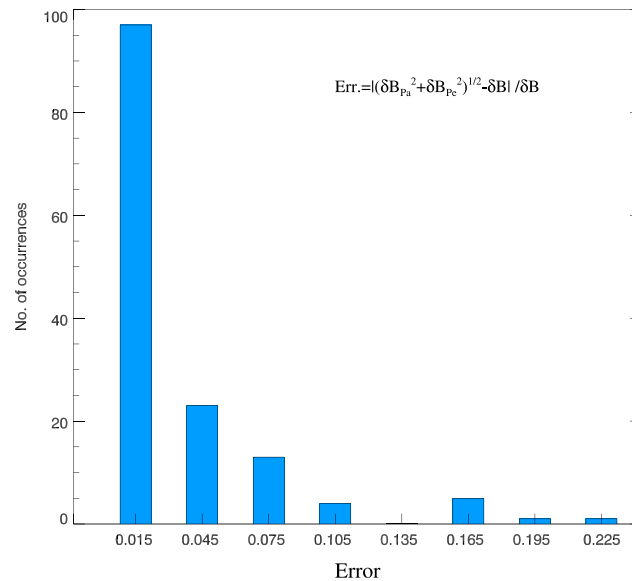


Figure 9. Histogram of the error on the computed parallel and transverse wave amplitudes shown in Figure 8.

parallel amplitudes in the range from ~ 0 to ~ 0.3 , while most waves ($\sim 89\%$) have a larger range of relative perpendicular amplitudes from ~ 0.1 to ~ 1.0 ; i.e., most waves have larger perpendicular (transverse) amplitudes compared to parallel (compressional) amplitudes. The ratio of parallel to perpendicular components distribution is shown in Figure 8 (bottom), which is as expected similar to the ratio of compressional to transverse power distribution as shown on Figure 4.

4. Discussion and Conclusions

Earlier reports revealed the existence of ULF waves upstream of the Venus bow shock [Russell and Hoppe, 1983; Orłowski *et al.*, 1995; Shan *et al.*, 2014]. For the present work, a statistical study of Venesian foreshock ULF wave

properties is undertaken using 1 Hz VEX-MAG data. The study is restricted to wave trains that appear quasi-monochromatic having an unambiguous frequency peak in the power spectrum. Based on a bow shock model from Shan *et al.* [2015], the ULF wave events are localized within the Venesian foreshock. Our statistics is based on 157 quasi-monochromatic wave events identified with a frequency far below the local proton gyrofrequency. The observations indicate that the selected wave events are found within the entire foreshock region that the spacecraft can explore; most of the cases are observed upstream of the terminator plane. Precisely, the quasi-monochromatic ULF waves mainly appear in the upstream region of a quasi-parallel shock. Moreover, the ULF waves occur up to a large radial distance $\sim 12 R_V$ from the center of planet. These results are very different from those obtained from the investigation of proton cyclotron waves. The ULF waves in the present study are always limited to the foreshock region, on contrary to proton cyclotron waves that are also observed when the spacecraft is not magnetically connected to the bow shock [Delva *et al.*, 2015].

For each selected case the wave period, power spectrum of the compressional and transverse components, polarization, propagation angle, and amplitude are determined. Our results show that most of the waves ($\sim 62\%$) have 20–30 s wave period, which is about 2–3 times T_{cp} . The average period is about 27 s in the spacecraft frame very similar to the average wave period seen in the foreshock of Earth [Eastwood *et al.*, 2005a]. This is consistent with the foreshock wave relationship shown in an earlier study [Hoppe and Russell, 1982], due to the different strength of IMF at different planets. The spread in the wave periods (Figure 4) may result from the variation of solar wind speed, because the waves are convected by the solar wind flow and Doppler shift is significant [Hoppe and Russell, 1983; Russell and Hoppe, 1983; Mazelle *et al.*, 2003; Eastwood *et al.*, 2005a] as shown from the histogram of the angle θ_{kx} (Figure 6).

Since the plasma data are not available, an accurate determination of the wavelength is not possible. However, for a typical solar wind velocity the wavelength can be estimated to one Venesian radius. Another wave feature regards the transverse component which dominates the wave power contrary to the nonlinear waves like steepened magnetosonic and shocklets, which have large compressional components and are excluded from the present study. In the downstream region of the Venesian bow shock, low-frequency fluctuations are mainly dominated by the transverse power [Du *et al.*, 2010]. Perhaps, these waves seen downstream mainly come from the foreshock [Luhmann *et al.*, 1983; Shan *et al.*, 2014] because their phase velocity is lower than the solar wind speed.

In a previous study used the mapping of the standard deviations of the magnetic field components and magnitude from more than 700,000 time intervals within nominal Parker spiral region (IMF cone angle from

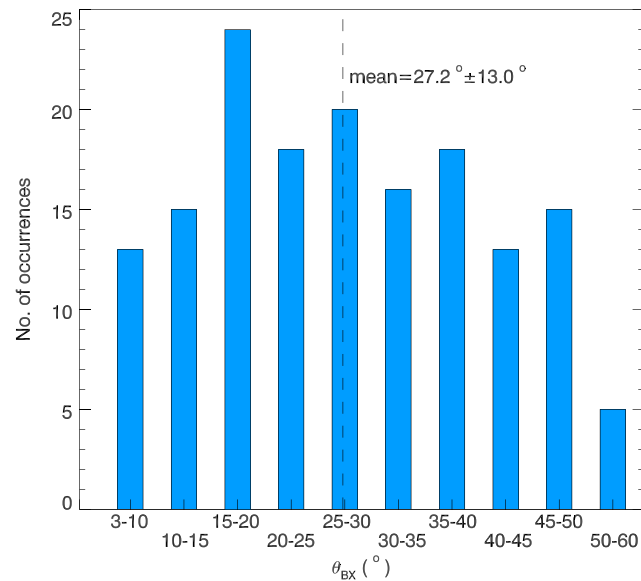


Figure 10. Histogram of IMF cone angles for the 157 ULF wave subintervals.

25° to 45°) to infer the ULF wave activity, which appear confined to the nose of the shock [Crawford *et al.*, 1998, their plate 2]. But their study was not limited to quasi-monochromatic ULF waves and can also introduce many other solar wind or foreshock transients, which can impact the variance. In the present study, the IMF cone angle for 157 subintervals has a large range from 0° to 60° (Figure 10). The mean value is $27.2^\circ \pm 13.0^\circ$, which indicates a lower value than the nominal range of Parker spiral angles at Venus (25°–45°). A judicious localization of wave events requires the use of the solar foreshock coordinates system [Greenstadt and Baum, 1986] because the occurrence is cone angle-dependent.

Based on MVA results, we found that most of ULF waves show a nearly circular or slightly elliptical polarization ($\lambda_i/\lambda_j < 3$) with propagation angles mainly less than 30°, with a mean value $22.5^\circ \pm 15.6^\circ$. Again, these results are very similar to those found inside the Earth's foreshock [Eastwood *et al.*, 2005b]. The small propagation angles strongly indicate that those ULF waves are excited by backstreaming ions propagating sunward along the IMF. Both theory and observations suggest that the backstreaming ions are connected to the generation of ULF waves [Gary, 1991; Hoppe and Russell, 1982; Meziane *et al.*, 2001; Mazelle *et al.*, 2003], particularly, the growth rate of the ion-ion beam instability is maximized for parallel propagation [Gary *et al.*, 1981]. Similar values of the propagation angle are found in the upstream region for the case studies of waves transmitted through the quasi-parallel shock by Shan *et al.* [2014].

Moreover, although the quasi-monochromatic ULF waves are seen on IMF lines making an angle θ_{Bn} between 0° and 80°, most of the cases are associated with a quasi-parallel geometry (mean $\theta_{Bn} = 31^\circ$). We should, however, emphasize that the large value of θ_{Bn} angles ($\sim 80^\circ$) are entailed with significant errors given that the bow shock model is quite poor at the flanks. Although the results is bow shock model-dependent, our results is in good agreement with an earlier study for the Earth's case carried out by Le and Russell [1992b], showing that ULF waves are confined in the foreshock region with $\theta_{Bn} \leq 50^\circ$. In addition, we studied the parallel and perpendicular amplitudes for the ULF wave cases. We found that most of the waves have small relative parallel wave amplitudes (less than 0.3), while the perpendicular amplitudes are larger, 0.1–1.0 B_o , a result that is consistent with small propagation angles with respect to the background field.

Based on the properties found in the present study, it is strongly suggested that the quasi-monochromatic ULF waves seen upstream of the Venusian bow shock are excited by foreshock backstreaming ions with a process similar to the one operating in the terrestrial foreshock. From ISEE 2 observations at the Earth, $\sim 83\%$ of field-aligned beams are in the foreshock with $\theta_{Bn} > 26^\circ$ [Bonifazi and Moreno, 1981]. The shock normal angles found here for $\sim 55\%$ wave cases are larger than 26°.

The study of the association of Venusian foreshock ULF waves with backstreaming ion velocity distributions is certainly necessary to understand the wave excitation mechanism. A possible route is to investigate the existence of an ULF boundary beyond which the IMF fluctuations occur. Such boundaries have been reported in the case of the Earth [Greenstadt *et al.*, 1986; Meziane and d'Uston, 1998; Andrés *et al.*, 2015] and Saturn [Andrés *et al.*, 2015]. Using PVO data, a preliminary investigation of Venus foreshock ULF boundary has been initiated by Greenstadt *et al.* [1987], and it is certainly suitable to pursue this investigation with VEX-MAG data. This is the scope of a future work.

Acknowledgments

The authors would like to thank the VEX MAG team for providing data sets used in this study. All the magnetic field data are obtained from T. Zhang (e-mail: Tielong.zhang@oeaw.ac.at). L.S. thanks E. Penou for his assistance. L.S. was supported by the National Science Foundation of China (grant 41504134), a project funded by China Postdoctoral Science Foundation, and CAS Key Laboratory of Geospace Environment, University of Science and Technology of China. Work at USTC is supported by the National Science Foundation of China (grants 41331067, 41274144, 41174124, and 41121003) and 973 Program (grants 2013CBA01503 and 2012CB825602). Work at IGGCAS is supported by the National Basic Research Program of China (grant 2014CB845903) and the National Natural Science Foundation of China (grants 41174122 and 41474144).

References

- Andrés, N., D. O. Gómez, C. Bertucci, C. Mazelle, and M. K. Dougherty (2013), Saturn's ULF wave foreshock boundary: Cassini observations, *Planet. Space Sci.*, *79*–*80*, 64–75, doi:10.1016/j.pss.2013.01.014.
- Andrés, N., K. Meziane, C. Mazelle, C. Bertucci, and D. Gómez (2015), The ULF wave foreshock boundary: Cluster observations, *J. Geophys. Res. Space Physics*, *120*, 4181–4193, doi:10.1002/2014JA020783.
- Bertucci, C., N. Achilleos, C. Mazelle, G. B. Hospodarsky, M. Thomsen, M. K. Dougherty, and W. Kurth (2007), Low-frequency waves in the foreshock of Saturn: First results from Cassini, *J. Geophys. Res.*, *112*, A09219, doi:10.1029/2006JA012098.
- Blanco-Cano, X., G. Le, and C. T. Russell (1999), Identification of foreshock waves with 3-s periods, *J. Geophys. Res.*, *104*, 4643–4656, doi:10.1029/1998JA900103.
- Blanco-Cano, X., N. Omid, and C. T. Russell (2006a), Macrostructure of collisionless bow shocks: 2. ULF waves in the foreshock and magnetosheath, *J. Geophys. Res.*, *111*, A10205, doi:10.1029/2005JA011421.
- Blanco-Cano, X., N. Omid, and C. T. Russell (2006b), ULF waves and their influence on bow shock and magnetosheath structures, *Adv. Space Res.*, *37*, 1522–1531, doi:10.1016/j.asr.2005.10.043.
- Bonifazi, C., and G. Moreno (1981), Reflected and diffuse ions backstreaming from the Earth's bow shock 2. Origin, *J. Geophys. Res.*, *86*, 4405–4413, doi:10.1029/JA086iA06p04405.
- Burgess, D. (1987), Simulations of backstreaming ion beams formed at oblique shocks by direct reflection, *Ann. Geophys.*, *5*, 133–145.
- Burgess, D. (1997), What do we really know about upstream waves?, *Adv. Space Res.*, *20*(4/5), 673–682, doi:10.1016/S0273-1177(97)00455-9.
- Crawford, G. K., R. J. Strangeway, and C. T. Russell (1998), Statistical imaging of the Venus foreshock using VLF wave emissions, *J. Geophys. Res.*, *103*, 11,985–12,003, doi:10.1029/97JA02883.
- Delva, M., T. L. Zhang, M. Volwerk, W. Magnes, C. T. Russell, and H. Y. Wei (2008), First upstream proton cyclotron wave observations at Venus, *Geophys. Res. Lett.*, *35*, L03105, doi:10.1029/2007GL032594.
- Delva, M., C. Mazelle, C. Bertucci, M. Volwerk, Z. Vörös, and T. L. Zhang (2011), Proton cyclotron wave generation mechanisms upstream of Venus, *J. Geophys. Res.*, *116*, A02318, doi:10.1029/2010JA015826.
- Delva, M., C. Bertucci, M. Volwerk, R. Lundin, C. Mazelle, and N. Romanelli (2015), Upstream proton cyclotron waves at Venus near solar maximum, *J. Geophys. Res. Space Physics*, *120*, 344–354, doi:10.1002/2014JA020318.
- Du, J., T. L. Zhang, W. Baumjohann, C. Wang, M. Volwerk, Z. Vörös, and L. Guicking (2010), Statistical study of low-frequency magnetic field fluctuations near Venus under the different interplanetary magnetic field orientations, *J. Geophys. Res.*, *115*, A12251, doi:10.1029/2010JA015549.
- Eastwood, J. P., A. Balogh, E. A. Lucek, C. Mazelle, and I. Dandouras (2005a), Quasi-monochromatic ULF foreshock waves as observed by the four-spacecraft Cluster mission: 1. Statistical properties, *J. Geophys. Res.*, *110*, A11219, doi:10.1029/2004JA010617.
- Eastwood, J. P., A. Balogh, E. A. Lucek, C. Mazelle, and I. Dandouras (2005b), Quasi-monochromatic ULF foreshock waves as observed by the four-spacecraft Cluster mission: 2. Oblique propagation, *J. Geophys. Res.*, *110*, A11220, doi:10.1029/2004JA010618.
- Fuselier, S. A. (1995), Ion distributions in the Earth's foreshock upstream from the bow shock, *Adv. Space Res.*, *15*(8–9), 43–52, doi:10.1016/0273-1177(94)00083-D.
- Gary, S. P. (1991), Electromagnetic ion/ion instabilities and their consequences in space plasmas: A review, *Space Sci. Res.*, *56*, 373–415.
- Gary, S. P., J. T. Gosling, and D. W. Forslund (1981), The electromagnetic ion beam instability upstream of the Earth's bow shock, *J. Geophys. Res.*, *86*, 6691–6696, doi:10.1029/JA086iA08p06691.
- Gedalin, M., M. Liverts, and M. A. Balikhin (2008), Distribution of escaping ions produced by non-specular reflection at the stationary quasi-perpendicular shock front, *J. Geophys. Res.*, *113*, A05101, doi:10.1029/2007JA012894.
- Gosling, J. T., J. R. Ashridge, S. J. Bame, G. Paschmann, and N. Sckopke (1978), Observations of two distinct populations of bow shock ions in the upstream solar wind, *Geophys. Res. Lett.*, *5*, 957–960, doi:10.1029/GL005i011p00957.
- Gosling, J. T., M. F. Thomsen, S. J. Bame, W. C. Feldman, G. Paschmann, and N. Sckopke (1982), Evidence for specularly reflected ions upstream from the quasi-parallel shock, *Geophys. Res. Lett.*, *9*, 1333–1336, doi:10.1029/GL009i012p01333.
- Greenstadt, E. W., and L. W. Baum (1986), Earth's compressional foreshock boundary revisited: Observations by the ISEE 1 magnetometer, *J. Geophys. Res.*, *91*, 9001–9006, doi:10.1029/JA091iA08p09001.
- Greenstadt, E. W., L. W. Baum, K. F. Jordan, and C. T. Russell (1987), The compressional ULF foreshock boundary of Venus: Observations by the PVO magnetometer, *J. Geophys. Res.*, *92*, 3380–3384, doi:10.1029/JA092iA04p03380.
- Greenstadt, E. W., G. Le, and R. J. Strangeway (1995), ULF waves in the foreshock, *Adv. Space Res.*, *15*(8–9), 71–84, doi:10.1016/0273-1177(94)00087-H.
- Hoppe, M. M., and C. T. Russell (1982), Particle acceleration at planetary bow shock waves, *Nature*, *295*, 41–42, doi:10.1038/295041a0.
- Hoppe, M. M., and C. T. Russell (1983), Plasma rest frame frequencies and polarizations of the low-frequency upstream waves: ISEE 1 and 2 observations, *J. Geophys. Res.*, *88*, 2021–2028, doi:10.1029/JA088iA03p02021.
- Hoppe, M. M., C. T. Russell, L. A. Frank, T. E. Eastman, and E. W. Greenstadt (1981), Upstream hydromagnetic waves and their association with backstreaming ion populations: ISEE-1 and -2 observations, *J. Geophys. Res.*, *86*, 4471–4492, doi:10.1029/JA086iA06p04471.
- Hoshino, M., and T. Terasawa (1985), Numerical study of the upstream wave excitation mechanism: 1. Nonlinear phase bunching of beam ions, *J. Geophys. Res.*, *90*, 57–64, doi:10.1029/JA090iA01p00057.
- Kucharek, H., E. Möbius, M. Scholer, C. Moukikis, L. Kistler, T. Horbury, A. Balogh, H. Réme, and J. Bosqued (2004), On the origin of field-aligned beams at the quasi-perpendicular bow shock: Multi-spacecraft observations by Cluster, *Ann. Geophys.*, *22*, 2301–2308, doi:10.5194/angeo-22-2301-2004.
- Le, G., and C. T. Russell (1992a), A study of ULF wave foreshock morphology—II: Spatial variation of ULF waves, *Planet. Space Sci.*, *40*(9), 1215–1225, doi:10.1016/0032-0633(92)90078-3.
- Le, G., and C. T. Russell (1992b), A study of ULF wave foreshock morphology—I: ULF foreshock boundary, *Planet. Space Sci.*, *40*(9), 1203–1213, doi:10.1016/0032-0633(92)90077-2.
- Le, G., and C. T. Russell (1994), The morphology of ULF waves in the Earth's foreshock, in *Solar Wind Sources of Magnetospheric Ultra-Low-Frequency Waves*, *Geophys. Monogr. Ser.*, vol. 81, edited by M. J. Engebretson, K. Takahashi, and M. Scholer, pp. 87–98, AGU, Washington, D. C.
- Le, G., P. J. Chi, X. Blanco-Cano, S. Boardsen, J. A. Slavin, and B. J. Anderson (2013), Upstream ultra-low frequency waves in Mercury's foreshock region: MESSENGER magnetic field observations, *J. Geophys. Res. Space Physics*, *118*, 2809–2823, doi:10.1002/jgra.50342.
- Lu, Q. M., L. D. Xia, and S. Wang (2006), Hybrid simulations of parallel and oblique electromagnetic alpha/proton instabilities in the solar wind, *J. Geophys. Res.*, *111*, A09101, doi:10.1029/2006JA011752.
- Lu, Q. M., A. M. Du, and X. Li (2009), Two-dimensional hybrid simulations of the oblique electromagnetic alpha/proton instability in the solar wind, *Phys. Plasmas*, *16*, 042901, doi:10.1063/1.3116651.

- Luhmann, J. G., M. Tatrallyay, C. T. Russell, and D. Winterhalter (1983), Magnetic field fluctuations in the Venus magnetosheath, *Geophys. Res. Lett.*, *10*, 655–658, doi:10.1029/GL010i008p00655.
- Mazelle, C., D. Le Quéau, and K. Meziane (2000), Nonlinear wave-particle interaction upstream from the Earth's bow shock, *Nonlinear Proc. Geophys.*, *7*, 185–190, doi:10.5194/npg-7-185-2000.
- Mazelle, C., et al. (2003), Production of gyrating ions from nonlinear wave-particle interaction upstream from the Earth's bow shock: A case study from Cluster-CIS, *Planet. Space Sci.*, *51*, 785–795, doi:10.1016/j.pss.2003.05.002.
- Mazelle, C., et al. (2004), Bow shock and upstream phenomena at Mars, *Space Sci. Res.*, *111*, 115–181.
- Mazelle, C., K. Meziane, M. Wilber, and D. Le Quéau (2005), Field-aligned and gyrating ion beams in a planetary foreshock, *AIP Conf. Proc.* *781*, 89, doi:10.1063/1.2032680.
- Mazelle, C., K. Meziane, M. Wilber, and D. Le Quéau (2007), Wave-particle interaction in the terrestrial ion foreshock: New results from Cluster, *AIP Conf. Proc.*, *932*, 175, doi:10.1063/1.2778961.
- McPherron, R. L., C. T. Russell, and J. Coleman (1972), Fluctuating magnetic fields in the magnetosphere. II: ULF waves, *Space Sci. Rev.*, *13*(3), 411–454, doi:10.1007/BF00219165.
- Meziane, K., and C. d'Uston (1998), A statistical study of the upstream intermediate ion boundary in the Earth's foreshock, *Ann. Geophys.*, *16*, 125–133, doi:10.1007/s00585-998-0125-7.
- Meziane, K., C. Mazelle, R. P. Lin, D. Le Quéau, D. E. Larson, G. K. Parks, and R. P. Lepping (2001), Three-dimensional observations of gyrating ion distributions far upstream from the Earth's bow shock and their association with low-frequency waves, *J. Geophys. Res.*, *106*, 5731–5742, doi:10.1029/2000JA900079.
- Meziane, K., et al. (2004a), Simultaneous observations of field-aligned beams and gyrating ions in the terrestrial foreshock, *J. Geophys. Res.*, *109*, A05107, doi:10.1029/2003JA010374.
- Meziane, K., et al. (2004b), Bow shock specularly reflected ions in the presence of low-frequency electromagnetic waves: A case study, *Ann. Geophys.*, *22*, 1–11, doi:10.5194/angeo-22-2325-2004.
- Meziane, K., M. Wilber, C. Mazelle, G. K. Parks, and A. M. Hamza (2005), A review of field-aligned beams observed upstream of the bow shock, in *The Physics of Collisionless Shocks, 4th Annual IGPP International Astrophysics Conference*, vol. 781, edited by G. Li, G. P. Zank, and C. T. Russell, pp. 116–122, Am. Inst. of Phys., Palm Springs, Calif.
- Meziane, K., A. M. Hamza, M. Wilber, C. Mazelle, and M. A. Lee (2013), On the field-aligned beam thermal energy, *J. Geophys. Res. Space Physics*, *118*, doi:10.1002/2013JA019060.
- Orlowski, D. S., G. K. Crawford, and C. R. Russell (1990), Upstream waves at Mercury, Venus and Earth: Comparison of the properties of one Hertz waves, *Geophys. Res. Lett.*, *17*(13), 2293–2296, doi:10.1029/GL017i013p02293.
- Orlowski, D. S., C. T. Russell, D. Krauss-Varban, and N. Omidi (1994), A test of the Hall-MHD model: Application to low-frequency upstream waves at Venus, *J. Geophys. Res.*, *99*, 169–178, doi:10.1029/93JA01808.
- Orlowski, D. S., C. T. Russell, D. Krauss-Varban, and N. Omidi (1995), Properties of ultralow frequency upstream waves at Venus and Saturn: A comparison, *Adv. Space Res.*, *16*, 143–148, doi:10.1016/0273-1177(95)00221-Y.
- Paschmann, G., N. Sckopke, J. R. Asbridge, S. J. Bame, and J. T. Gosling (1980), Energization of solar wind ions by reflection from the Earth's bow shock, *J. Geophys. Res.*, *85*, 4689–4693, doi:10.1029/JA085iA09p04689.
- Paschmann, G., N. Sckopke, I. Papamastorakis, J. R. Asbridge, S. J. Bame, and J. T. Gosling (1981), Characteristics of reflected and diffuse ions upstream from the Earth's bow shock, *J. Geophys. Res.*, *86*, 4355–4364, doi:10.1029/JA086iA06p04355.
- Rankin, D., and R. Kurtz (1970), Statistical study of micropulsation polarizations, *J. Geophys. Res.*, *75*, 5444–5458, doi:10.1029/JA075i028p05444.
- Russell, C. T., and M. M. Hoppe (1983), Upstream waves and particles, *Space Sci. Rev.*, *34*, 155–172, doi:10.1007/BF00194624.
- Russell, C. T., J. G. Luhmann, and R. J. Strangeway (2006), The solar wind interaction with Venus through the eyes of the Pioneer Venus Orbiter, *Planet. Space Sci.*, *54*, 1482–1495, doi:10.1016/j.pss.2006.04.025.
- Savoini, P., and B. Lembège (2015), Production of nongyrotropic and gyrotropic backstreaming ion distributions in the quasi-perpendicular ion foreshock region, *J. Geophys. Res. Space Physics*, *120*, 7154–7171, doi:10.1002/2015JA021018.
- Scholer, M. (1995), Interaction of upstream diffuse ions with the solar wind, *Adv. Space Res.*, *15*(8–9), 125–135, doi:10.1016/0273-1177(94)00094-H.
- Shan, L., Q. Lu, M. Wu, X. Gao, C. Huang, T. Zhang, and S. Wang (2014), Transmission of large-amplitude ULF waves through a quasi-parallel shock at Venus, *J. Geophys. Res. Space Physics*, *119*, 237–245, doi:10.1002/2013JA019396.
- Shan, L., Q. Lu, C. Mazelle, C. Huang, T. Zhang, M. Wu, X. Gao, and S. Wang (2015), The shape of the Venusian bow shock at solar minimum and maximum: Revisit based on VEX observations, *Planet. Space Sci.*, *109–110*, 32–37, doi:10.1016/j.pss.2015.01.004.
- Sonnerup, B. U. Ö., and M. Scherble (1998), Minimum and maximum variance analysis, in *Analysis Methods for Multi-Spacecraft Data. ISSI Scientific Reports*, edited by G. Paschmann and P. W. Daly, pp. 185–220, ESA Publications Div., Noordwijk, Netherlands.
- Su, Y., Q. Lu, C. Huang, M. Wu, X. Gao, and S. Wang (2012), Particle acceleration and generation of diffuse superthermal ions at a quasi-parallel collisionless shock: Hybrid simulations, *J. Geophys. Res.*, *117*, A08107, doi:10.1029/2012JA017736.
- Thomsen, M. F., J. T. Gosling, and S. J. Bame (1985), Gyrating ions and large-amplitude monochromatic MHD waves upstream of the Earth's bow shock, *J. Geophys. Res.*, *90*, 267–273, doi:10.1029/JA090iA01p00267.
- Wilson, L. B., III (2016), Low-frequency waves at and upstream of collisionless shocks, in *Low-Frequency Waves in Space Plasmas*, *Geophys. Monogr. Ser.*, chap. 16, edited by A. Keiling, D. H. Lee, and V. Nakariakov, pp. 269–291, AGU, Hoboken, N. J.
- Wilson, L. B., III, C. A. Cattell, P. J. Kellogg, K. Goetz, K. Kersten, J. C. Kasper, A. Szabo, and K. Meziane (2009), Low-frequency whistler waves and shocklets observed at quasi-perpendicular interplanetary shocks, *J. Geophys. Res.*, *114*, A10106, doi:10.1029/2009JA014376.
- Wilson, L. B., III, A. Koval, D. G. Sibeck, A. Szabo, C. A. Cattell, J. C. Kasper, B. A. Maruca, M. Pulupa, C. S. Salem, and M. Wilber (2013), Shocklets, SLAMS, and field-aligned ion beams in the terrestrial foreshock, *J. Geophys. Res. Space Physics*, *118*, 957–966, doi:10.1029/2012JA018186.
- Winske, D., and M. M. Leroy (1984), Diffuse ions produced by electromagnetic ion beam instabilities, *J. Geophys. Res.*, *89*, 2673–2688, doi:10.1029/JA089iA05p02673.
- Winske, D., and K. B. Quest (1986), Electromagnetic ion beam instabilities: Comparison of one- and two-dimensional simulations, *J. Geophys. Res.*, *91*, 8789–8797, doi:10.1029/JA091iA08p08789.
- Zhang, T. L., et al. (2006), Magnetic field investigation of the Venus plasma environment: Expected new results from Venus Express, *Planet. Space Sci.*, *54*, 1336–1343, doi:10.1016/j.pss.2006.04.018.